Received: 14 November 2017 | Revised: 4 January 2018 | Accepted: 5 January 2018

DOI: 10.1002/ddr.21422

RESEARCH ARTICLE

WILEY DDR

Ursolic acid derivatives as potential antidiabetic agents: *In vitro*, *in vivo*, and *in silico* studies

Ricardo Guzmán-Ávila[1] | Virginia Flores-Morales[2*] | Paolo Paoli[3] | Guido Camici[3] | Juan José Ramírez-Espinosa[4] | Litzia Cerón-Romero[1] | Gabriel Navarrete-Vázquez[1] | Sergio Hidalgo-Figueroa[5] | Maria Yolanda Rios[6] | Rafael Villalobos-Molina[7] | Samuel Estrada-Soto[1]

Enabling Technologies		Strategy, Management & Health Policy	
Hit, Lead & Candidate Discovery	Preclinical Research & Development	Clinical Research	Post-Market Research

[1]Facultad de Farmacia, Universidad Autónoma del Estado de Morelos, Cuernavaca, Morelos 62209, Mexico

[2]Laboratorio de Síntesis Asimétrica y Bioenergética (LSAyB), Unidad Académica de Ciencias Químicas, Universidad Autónoma de Zacatecas, Zacatecas, Zacatecas 98160, Mexico

[3]Dipartimento di Scienze Biomediche Sperimentali e Cliniche "Mario Serio", Sezione di Scienze Biochimiche, Universitá degli Studi di Firenze, Firenze 50134, Italy

[4]Instituto de Ciencias Biomédicas, Universidad Autónoma de Ciudad Juárez, Juárez, Chihuahua 32310, Mexico

[5]Cátedras CONACyT IPICYT/Consorcio de Investigación, Innovación y Desarrollo para las Zonas Áridas, San Luis Potosí 78216, Mexico

[6]Centro de Investigaciones Químicas, IICBA, Universidad Autónoma del Estado de Morelos, Cuernavaca, Morelos 62209, Mexico

[7]Unidad de Biomedicina, Facultad de Estudios Superiores Iztacala, Universidad Nacional Autónoma de México, Tlalnepantla, Estado de México 54090, México

Correspondence
Dr. Samuel Estrada-Soto
Email: enoch@uaem.mx

Abstract

Protein tyrosine phosphatase 1B (PTP-1B) has attracted interest as a novel target for the treatment of type 2 diabetes, this because its role in the insulin-signaling pathway as a negative regulator. Thus, the aim of current work was to obtain seven ursolic acid derivatives as potential antidiabetic agents with PTP-1B inhibition as main mechanism of action. Furthermore, derivatives **1**–**7** were submitted *in vitro* to enzymatic PTP-1B inhibition being **3, 5,** and **7** the most active compounds (IC_{50} = 5.6, 4.7, and 4.6 μM, respectively). In addition, results were corroborated with *in silico* docking studies with PTP-1B orthosteric site A and extended binding site B, showed that **3** had polar and Van der Waals interactions in both sites with Lys120, Tyr46, Ser216, Ala217, Ile219, Asp181, Phe182, Gln262, Val49, Met258, and Gly259, showing a docking score value of −7.48 Kcal/mol, being more specific for site A. Moreover, compound **7** showed polar interaction with Gln262 and Van der Waals interactions with Ala217, Phe182, Ile219, Arg45, Tyr46, Arg47, Asp48, and Val49 with a predictive docking score of −6.43 kcal/mol, suggesting that the potential binding site could be localized in the site B adjacent to the catalytic site A. Finally, derivatives **2** and **7** (50 mg/kg) were selected to establish their *in vivo* antidiabetic effect using a noninsulin-dependent diabetes mice model, showing significant blood glucose lowering compared with control group ($p < .05$).

KEYWORDS

antidiabetic agents, docking, pentacyclic acid triterpenes, PTP-1B inhibition, ursolic acid derivatives

*The same level of participation as the principal and correspondence author is considered.

1 | INTRODUCTION

According to the World Health Organization, the chronic degenerative diseases represent the main causes of death in the world. Diabetes is a metabolic disease, which is characterized by an impaired regulation of glucose, and additionally, lipids and proteins (Mahapatra, Asati, & Bharti, 2015). This because insulin is not able to perform its function as main metabolic regulator in peripheral tissues, because of lack of insulin (type 1 diabetes) or because of resistance to insulin action and/or impaired insulin secretion (type 2 diabetes). Diabetes increases the risk to develop micro and macrovascular complications such as neuropathy, nephropathy and retinopathy, triggering consequences like cardiovascular diseases (myocardial infarction, stroke, among others), blindness, limb amputation, and end-stage renal disease (Brownlee, 2001). Moreover, diabetes has been linked to central nervous system diseases like depression and cognition disturbances (Li, Zhang, & Sima, 2007).

Despite the availability of drugs for the treatment of diabetes, many of them fail because two frequent reasons (Tahrani, Bailey, Del Prato, & Barnett, 2011): (a) many drugs cause diverse side-effects, that is, hypoglycemia, edema, weight gain, increasing cardiovascular risk, which can limit its use for the patient; (b) the improvement in the control of glycaemia is not continuous, due to the degenerative features related with the disease, thus, eventually it is necessary to increase the dose of the drug used or combinatorial therapy is needed to increase control. Thus, currently it is necessary to develop new drugs that counteract these points, and/or to obtain novel drugs which act at new targets. In this context, protein tyrosine phosphatase 1B (PTP-1B) has recently shown an important influence over insulin sensitivity, since it is implicated in modulating insulin signal transduction becoming a key regulator of insulin-receptor activity, and downstream signaling pathways (Johnson, Ermolieff, & Jirousek, 2002). This is related with a dephosphorylation of active insulin receptor (IR) (Romsicki, Reece, Gauthier, Asante-Appiah, & Kennedy, 2004). Also, PTP-1B is implicated in the regulation of the leptin receptor, which is involved in food intake regulation by CNS (Klok, Jakobsdottir, & Drent, 2007). PTP-1B is an enzyme formed by 435 amino acids residues, which is anchored into cytoplasmic face of endoplasmic reticulum (Johnson et al., 2002) and presents two important regions, sites A (catalytic) and B (extended binding pocket). The A site is formed by 214–221 residues and catalyzes the dephosphorilation of tyrosine arylphosphate residues (Tonks, 2003). The second region (B site), is an extended binding site but inactive region next to A site, which only binds to arylphosphate groups (Puius et al., 1997). Then, inhibition of PTP-1B could be a very important target to develop new antidiabetic drugs. There are several synthetic and natural derived compounds which are described as PTP-1B inhibitors (Verma, Gupta, Chaudhary, & Garg, 2017).

Natural products represent a great source for to study and develop new drugs candidates for the treatment of diabetes (Liu, Chen, Hu, Guo, & Shen, 2010). Ursolic acid (UA) is a triterpene that has shown metabolic (Sheng & Sun, 2011), cardiovascular (Aguirre-Crespo et al., 2006; Rios et al., 2012; Somova, Nadar, Rammanan, and Shode, 2003a; Somova, Shode, Ramnanan, & Nadar, 2003b), antibacterial (Nascimento et al., 2014), antifungal (Innocente et al., 2014), cytotoxic (Li et al., 2014), antidepressant (Colla et al., 2014; Machado et al., 2012), antioxidant and antiatherogenic effects (Allouche, Beltrán, Gaforio, Uceda, & Mesa, 2010), among others, which makes it an important scaffold in medicinal chemistry. Currently, is known that the ursolic acid antidiabetic effect is mediated by its interaction with different targets: UA acts as insulinomimetic (Jung et al., 2007), increasing the autophosphorylation and activation of insulin receptor, and also proceeds as insulin sensitizer since it is able to inhibit the PTP-1B enzyme (Ramírez-Espinosa et al., 2011; Zhang et al., 2006). A recent report showed that UA augments GLUT4 as a result of increasing intracellular Ca^{2+} concentration, which augments movement and translocation of GLUT4 transporter unto membrane (Castro et al., 2015). Other UA direct and indirect antidiabetic mechanisms are enzymatic inhibition of: 11β-HSD1 (Rollinger et al., 2010), glycogen phosphorylase (Jang, Kim, Choi, Kwon, & Lee, 2010), α-glucosidase (Wu, Zhang, Lu, He, & Zhao, 2014), and aldose reductase (Lee et al., 2014). Thus, the aim of current work was to synthesize new UA derivatives based on this scaffold in order to discover more potent, specific and effective antidiabetic bioactive compounds.

2 | METHODS AND MATERIALS

2.1 | General

The preparation of **1**–**6** UA derivatives was carried out in a CEM Discovery BenchMate system with a potency of 100 W. The temperature reaction was set at 60°C under open vessel system. Reaction progress and purity of products was monitored by thin layer chromatography (TLC) using silica gel 60 F_{254} aluminum sheets, visualizing the plates under UV-light and then spraying with $(NH_4)Ce(SO_4)_4$ in 2N H_2SO_4 and heating. The products were purified by flash column chromatography (FCC) using 40–63 μm silica gel (230–440 mesh). Melting points were determined on a Fisher–Johns apparatus and are reported uncorrected.

^1H, ^{13}C, and bidimensional spectra were recorded on Varian unity 400^{TM} spectrometer equipped with a 5 mm inverse detection pulse field gradient probe at 25°C at 400 MHz for ^1H and 100 MHz for ^{13}C. Chemical shifts are given in values of part per million, referenced to tetramethylsilane (TMS) as an internal standard.

2.2 | Synthesis of ursolic acid derivatives

2.2.1 | Starting material

Ursolic acid was purchased from Sigma-Aldrich (St. Louis, MO). Chemical reagents were purchased analytical grade from Sigma-Aldrich, Mexico. Commercially available solvents (*n*-hexane, ethyl acetate, and acetone) were used after purification and dried according to standard procedures.

2.2.2 | Synthesis procedure for derivatives 1, 2, and 6

In a well-stirred and cooled solution of UA (1.0 equiv.) in dry THF was added 2.1 equiv. of the corresponding base. Mixture reaction was stirred at 0°C for 30 min. Alkyl halide (2.1 equiv.) was added dropwise

over period of 5 min, then the reaction mixture was placed under microwave radiation in CEM equipment at 60°C. Solvent was eliminated under vacuum and the reaction crude was purified by FCC.

(3β)-3-methoxyursen-12-en-28-oic acid (1)

UA 120 mg (0.263 mmol), THF (2 mL), Na 15.1 mg (0.657 mmol), methyl iodide 35 μL (0.552 mmol), 2 h reaction. FCC (*n*-hexane/acetone 90:10 v/v) affording 80.4 mg product, 65% yield, TLC: R_f = 0.41 (*n*-hexane/acetone 80:20 v/v); white powder; m.p. 165–167°C. ^{1}H-NMR (400 MHz, $CDCl_3$) δ 5.24 (t, ^3J = 3.6 Hz, 1H), 3.60 (s, 3H), 3.21 (dd, ^3J = 10.8, 4.8 Hz, 1H), 2.22 (d, ^3J = 10.7 Hz, 1H), 1.99 (td, ^3J = 13.3, 4.5 Hz, 1H), 1.90 (dd, ^3J = 8.9, 3.6 Hz, 2H), 1.76 (td, ^3J = 13.6, 4.6 Hz, 1H), 1.57 (m, 12H), 1.31 (m, 5H), 1.06 (s, 4H), 0.99 (d, 4H), 0.93 (dd, 6H), 0.85 (d, ^3J = 6.5 Hz, 3H), 0.73 (dd, 7H). ^{13}C-NMR (100 MHz, $CDCl_3$) δ 178.1 (C-28), 138.3 (C-13), 125.7 (C-12), 79.1 (C-3), 55.4 (C-5), 53.0 (C-18), 51.5 (C-A), 48.2 (C-17), 47.7 (C-9), 42.1 (C-14), 39.7 (C-8), 39.2 (C-19), 39.0 (C-20), 38.9 (C-4), 38.8 (C-1), 37.1 (C-10), 36.8 (C-22), 33.1 (C-7), 30.8 (C-21), 28.3 (C-23), 28.2 (C-15), 27.4 (C-2), 24.4 (C-16), 23.8 (C-27), 23.4 (C-11), 21.3 (C-30), 18.5 (C-6), 17.2 (C-26), 17.1 (C-29), 15.8 (C-25), 15.6 (C-24).

(3β)-3-ethoxyursen-12-en-28-oic acid (2)

UA 120 mg (0.263 mmol), THF (2 mL), Na° 15.1 mg (0.657 mmol), ethyl bromide 50 μL (0.552 mmol), 2 hours reaction. FCC (*n*-hexane/acetone 95:05 v/v) affording 113.4 mg product, 89% yield, TLC: R_f = 0.67 (*n*-hexane/acetone 80:20 v/v); white powder; m.p. 135–137°C. ^{1}H-NMR (400 MHz, $CDCl_3$) δ 5.23 (t, ^3J = 3.6 Hz, 1H), 4.04 (q, ^3J = 7.1 Hz, 2H), 3.20 (dd, ^3J = 10.9, 4.9 Hz, 1H), 2.23 (d, ^3J = 10.7 Hz, 1H), 1.97 (td, J = 13.3, 4.5 Hz, 1H), 1.89 (dt, ^3J = 8.8, 3.7 Hz, 2H), 1.77 (td, ^3J = 13.7, 4.6 Hz, 1H), 1.58 (m, 11H), 1.30 (m, 5H), 1.21 (t, ^3J = 7.1 Hz, 3H), 1.07 (s, 3H), 0.98 (s, 4H), 0.92 (m, 6H), 0.84 (d, ^3J = 6.5 Hz, 3H), 0.73 (dd, 7H). ^{13}C-NMR (100 MHz, $CDCl_3$) δ 177.7 (C-28), 138.4 (C-13), 125.7 (C-12), 79.3 (C-3), 60.2 (C-A), 55.5 (C-5), 53.1 (C-18), 48.1 (C-17), 47.8 (C-9), 42.3 (C-14), 39.8 (C-8), 39.3 (C-19), 39.1 (C-20), 39.0 (C-4), 38.9 (C-1), 37.2 (C-10), 36.9 (C-22), 33.3 (C-7), 30.9 (C-21), 28.4 (C-23), 28.2 (C-15), 27.5 (C-2), 24.4 (C-16), 23.7 (C-27), 23.5 (C-11), 21.4 (C-30), 18.5 (C-6), 17.3 (C-26), 17.2 (C-29), 15.8 (C-25), 15.7 (C-24), 14.4 (C-B).

Methyl (3β)-3-hydroxyursen-12-en-28-oate (6)

UA 120 mg (0.263 mmol), DCM (2 mL), DMF (1 mL), K_2CO_3 36.3 mg (0.263 mmol), methyl iodine 35 μL (0.552 mmol), 3 h reaction. FCC (*n*-hexane/ethyl acetate 90:10 v/v) affording 94.1 mg product, 76% yield; TLC: R_f = 0.55 (*n*-hexane/acetone 80:20 v/v); white powder; m.p. 172°C [Lit. 166–168°C] (Cerón-Romero et al., 2016). ^{1}H-NMR (400 MHz, $CDCl_3$) δ 5.24 (t, ^3J = 3.6 Hz, 1H), 3.60 (s, 3H), 3.21 (dd, ^3J = 10.9, 4.9 Hz, 1H), 2.23 (d, ^3J = 11.3 Hz, 1H), 2.00 (td, ^3J = 13.3, 4.5 Hz, 1H), 1.91 (dd, ^3J = 8.9, 3.7 Hz, 2H), 1.76 (td, ^3J = 13.7, 4.5 Hz, 1H), 1.58 (m, 12H), 1.31 (m, 5H), 1.05 (m, 4H), 0.98 (d, 4H), 0.92 (dd, 6H), 0.85 (t, ^3J = 6.5 Hz, 3H), 0.77 (d, 3H), 0.72 (m, 4H). ^{13}C-NMR (100 MHz, $CDCl_3$) δ 178.2 (C-28), 138.3 (C-13), 125.8 (C-12), 79.2 (C-3), 55.4 (C-5), 53.1 (C-18), 51.6 (C-A), 48.3 (C-17), 47.8 (C-9), 42.2 (C-14), 39.7 (C-8), 39.3 (C-19), 39.1 (C-20), 38.9 (C-4), 38.8 (C-1), 37.2 (C-10), 36.8 (C-22), 33.2 (C-7), 30.9 (C-21), 28.3 (C-23), 28.2 (C-15), 27.4 (C-2), 24.4 (C-16), 23.8 (C-27), 23.5 (C-11), 21.4 (C-30), 18.5 (C-6), 17.2 (C-26), 17.1 (C-29), 15.8 (C-25), 15.6 (C-24).

2.2.3 | Synthesis procedure for compound 3, 4, and 5

In a well-stirred and cooled solution of UA (1.0 equiv.) in dry CH_2Cl_2 and DMF was added 2.1 equiv. of the corresponding base. Mixture reaction was stirred at 0°C for 30 min. Acyl halide (2.1 equiv.) was added dropwise over a 5 min period, then, the reaction mixture was placed under microwave radiation in CEM equipment at 60°C. Solvent was eliminated under vacuum and the reaction crude was purified by FCC.

(3β)-3-(acetyloxy)ursen-12-en-28-oic acid (3)

UA 61.3 mg (0.134 mmol), DCM (2 mL), DMF (1 mL), Et_3N 40 μL (0.276 mmol), acetyl chloride 10 μL (0.144 mmol), 2 h reaction. FCC (*n*-hexane/ethyl acetate 90:10 v/v) affording 31.5 mg product, 48% yield, TLC: R_f = 0.35 (*n*-hexane/ethyl acetate 85:15 v/v); white powder; m.p. 185–187°C. [Lit. 175–178°C] (Collins et al., 2002). ^{1}H-NMR (400 MHz, $CDCl_3$): δ 5.16 (t, ^3J = 3.4 Hz, 1H), 4.43 (dd, ^3J = 9.3, 6.7 Hz, 1H), 2.11 (d, ^3J = 11.3, Hz, 1H), 1.98 (s, 3H), 1.92 (dd, ^3J = 13.2, 4.2 Hz, 1H), 1.84 (dd, ^3J = 8.8, 3.3 Hz, 2H), 1.78 (dd, ^3J = 13.6, 4.4 Hz, 1H), 1.61 (m, 6H), 1.43 (m, 4H), 1.24 (m, 5H), 1.02 (m, 5H), 0.88 (m, 6H), 0.79 (d, ^3J = 7.7 Hz, 9H), 0.69 (s, 3H). ^{13}C-NMR (100 MHz, $CDCl_3$): δ 184.3 (C-28), 171.3 (C-A), 138.1 (C-13), 125.9 (C-12), 81.1 (C-3), 55.5 (C-5), 52.7 (C-18), 48.2 (C-17), 47.6 (C-9), 42.1 (C-14), 39.7 (C-8), 39.2 (C-19), 39.0 (C-20), 38.4 (C-4), 37.9 (C-1), 37.1 (C-10), 36.9 (C-22), 33.0 (C-7), 30.8 (C-21), 28.3 (C-23), 28.2 (C-15), 24.2 (C-16), 23.8 (C-27), 23.5 (C-11), 21.5 (C-B), 21.4 (C-30), 18.3 (C-6), 17.3 (C-26), 17.2 (C-29), 16.9 (C-25), 15.7 (C-24).

(3β)-3-(formyloxy)ursen-12-en-28-oic acid (4)

UA 60.3 mg (0.134 mmol), DCM (2 mL), DMF (1 mL), K_2CO_3 36.3 mg (0.263 mmol), benzoyl chloride 20 μL (0.144 mmol), 2 h reaction. FCC (*n*-hexane/acetone 90:10 v/v) affording 37.5 mg product, 58% yield, TLC: R_f = 0.31 (*n*-hexane/acetone 90:10 v/v); white crystals; m.p. 120–121°C. [Lit. 117–119°C] (Collins et al., 2002). ^{1}H-NMR (400 MHz, $CDCl_3$) δ 8.11 (s, 1H), 5.23 (t, ^3J = 3.8 Hz, 1H), 4.62 (dd, ^3J = 9.8, 6.1 Hz, 1H), 2.18 (d, ^3J = 11.8 Hz, 1H), 2.01 (m, 1H), 1.92 (dd, ^3J = 8.8, 3.7 Hz, 2H), 1.85 (dd, ^3J = 13.6, 5.0 Hz, 1H), 1.68 (m, 6H), 1.50 (m, 4H), 1.32 (m, 7H), 1.09 (m, 5H), 0.96 (m, 6H), 0.86 (m, 9H), 0.77 (s, 2H). ^{13}C NMR (100 MHz, $CDCl_3$) δ 184.1 (C-28), 161.3 (C-A), 138.2 (C-13), 125.9 (C-12), 81.3 (C-3), 55.5 (C-5), 52.7 (C-18), 48.2 (C-17), 47.5 (C-9), 42.1 (C-14), 39.7 (C-8), 39.2 (C-19), 39.0 (C-20), 38.4 (C-4), 37.8 (C-1), 37.1 (C-10), 36.9 (C-22), 33.0 (C-7), 30.8 (C-21), 29.9 (C-23), 28.2 (C-15), 24.2 (C-2), 23.9 (C-16), 23.8 (C-27), 23.5 (C-11), 21.4 (C-30), 18.4 (C-6), 17.3 (C-26), 17.2 (C-29), 16.9 (C-25), 15.7 (C-24).

(3β)-3-[(2E)-but-2-enoyloxy]ursen-12-en-28-oic acid (5)

UA 120.6 mg (0.364 mmol), DCM (2 mL), DMF (1 mL), K_2CO_3 72.6 mg (0.526 mmol), crotonyl chloride 40 μL (0.288 mmol), 3 h reaction. FCC (*n*-hexane/ethyl acetate 90:10 v/v) affording 33.2 mg product, 24% yield, TLC: R_f = 0.52 (*n*-hexane/acetone 80:20 v/v); white powder; m.p.

189–192°C. ^{1}H-NMR (400 MHz, $CDCl_3$) δ 6.95 (dd, ^3J = 15.5, 6.9 Hz, 1H), 5.85 (dd, ^3J = 15.5, Hz, 1H), 5.24 (t, ^3J = 3.3 Hz, 1H), 4.55 (m, 1H), 1.87 (m, 5H), 1.68 (m, 6H), 1.55 (m, 4H), 1.34 (m, 5H), 1.25 (s, 3H), 1.17 (d, 1H), 1.08 (s, 4H), 0.96 (m, 7H), 0.87 (m, 10H), 0.78 (m, 3H). ^{13}C-NMR (100 MHz, $CDCl_3$) δ 183.6 (C-28), 166.6 (C-A), 144.2 (C-C), 138.2 (C-13), 126.0 (C-12), 123.6 (C-B), 80.8 (C-3), 55.5 (C-5), 52.8 (C-18), 48.2 (C-17), 47.7 (C-9), 42.1 (C-14), 39.7 (C-8), 39.2 (C-19), 39.0 (C-20), 38.5 (C-4), 38.1 (C-1), 37.1 (C-10), 37.0 (C-22), 33.1 (C-7), 30.7 (C-21), 29.9 (C-23), 28.3 (C-15), 24.3 (C-13), 24.1 (C-16), 23.8 (C-27), 23.5 (C-11), 21.4 (C-30), 18.4 (C-16), 17.3 (C-D), 17.2 (C-26), 17.0 (C-29), 16.9 (C-25), 15.8 (C-24).

(3β)-ursen-12-en-3,28-diol (7)

A cooled solution of $LiAlH_4$ (180 mg, 4.743 mmol) in dry THF (10 mL) was added dropwise to a mixture of UA (500 mg, 1.085 mmol) and dry THF (5 mL) under N_2 atmosphere. The mixture reaction was stirred at 0°C for 1 h. The reaction was refluxed 7 h. Reaction was quenched by addition of NaOH 10% (10 mL). Precipitate was filtered and washed with AcOEt (3 × 5 mL). The combined organic layers were dried over anhydrous Na_2SO_4, and evaporated under reduced pressure. FCC: (*n*-hexane:2-propanol, 98:02) affording 73.6 mg product, 15% yield. TLC: R_f = 0.47 (*n*-hexane: 2-propanol, 95:05); white powder; m.p. 218–221°C [Lit. 222–224°C] (Nascimento et al., 2014). ^{1}H-NMR (400 MHz, $CDCl_3$) δ 5.24 (t, ^3J = 3.7 Hz, 1H), 4.47 (dd, ^3J = 9.2, 3.4 Hz, 1H), 3.37 (m, 1H), 3.21 (m, 1H), 2.23 (m, 1H), 2.03 (m, 1H), 1.90 (m, 2H), 1.60 (m, 11H), 1.34 (m, 5H), 1.26 (s, 2H), 1.17 (s, 1H), 1.09 (m, 3H), 1.04 (s, 1H), 0.96 (m, 11H), 0.86 (m, 3H), 0.81 (s, 2H), 0.78 (m, 4H), 0.72 (m, 1H). ^{13}C-NMR (100 MHz, $CDCl_3$) δ 138.14 (C-13), 126.1 (C-12), 79.3 (C-3), 77.4 (C-28), 55.4 (C-5), 52.9 (C-18), 48.1 (C-17), 47.8 (C-9), 42.2 (C-14), 39.7 (C-8), 39.3 (C-19), 39.0 (C-20), 38.8 (C-1), 37.2 (C-10), 36.9 (C-22), 33.2 (C-7), 30.8 (C-21), 28.4 (C-23), 28.2 (C-15), 27.4 (C-2), 24.4 (C-16), 23.8 (C-27), 23.5 (C-11), 21.4 (C-30), 18.5 (C-6), 17.3 (C-26), 17.2 (C-29), 15.8 (C-25), 15.7 (C-24).

2.3 | Biological assays

2.3.1 | Expression and purification of recombinant PTP-1B

The human PTP-1B enzyme was purified as fusion protein from bacterial cell lines. The complete sequence of PTP-1B was cloned in the pGEX-2T bacterial expression vector downstream the GST sequence, and this vector was used to transform *E. coli* into TB1 strain. The recombinant fusion protein was purified from bacterial lysate using a single step affinity chromatography on glutathione-agarose. The solution with fusion protein was treated with thrombin for 3 h at 37°C. Then the active phosphatase was purified from GST and thrombin by gel filtration on a Superdex G75 column. The enzyme purity was determined by SDS-PAGE.

2.3.2 | PTP-1B inhibition assay

The assays were carried out at 37°C. The substrate (*p*NPP) was dissolved in 0.075 M of β,β-dimethyl glutarate pH 7.0 buffer, containing 1 mM EDTA and 1 mM dithiothreitol. The final volume was 1 mL. The reactions were started by adding aliquots of the enzyme and stopped with KOH 0.1M (4 mL) at the final time. The released *p*-nitrophenolate ion was determined by reading the absorbance at 400 nm (ε = 18,000 M^{-1} cm^{-1}).

To verify if compounds were reversible inhibitors, aliquots of PTP-1B were incubated in presence of at least 25-fold molar excess of inhibitor for 1 h at 37°C. Control experiments were performed adding DMSO instead of inhibitor. After this interval time, the enzyme solutions were diluted 400-fold and the residual enzyme activity was assayed.

2.4 | Animals

Male CD1 mice weighing 30–40 g body weight were housed at standard laboratory conditions and fed with a rodent pellet diet and water *ad libitum*. They were maintained at room temperature and a photoperiod of 12 h day/night cycle. Animals described as fasted were deprived of food for 16 h but had free access to water. All animals' procedures were conducted in accordance with Federal Regulations for Animals Experimentation and Care (SAGARPA, NOM-062-ZOO-1999), and approved by the Institutional Animal Health Care and Use Committee based on US National for Health publication (No. 85-23, revised 1985).

2.5 | Induction of NIDDM model

Streptozotocin (STZ, Sigma-Aldrich, St. Louis, MO) was dissolved in citrate buffer (pH 4.5), and nicotinamide (NAD) was dissolved in normal physiological saline solution. NIDDM was induced in overnight fasted mice by a single intraperitoneal injection of STZ (100 mg/kg), 15 min after the i.p. administration of NAD (40 mg/kg). After 10 days of STZ administration, blood glucose levels in each mouse was determined. Mice with >140 mg/dL glycaemia were considered diabetics (Hidalgo-Figueroa et al., 2017).

2.6 | *In vivo* antidiabetic assay

A described protocol was used (Chávez-Silva et al., 2018). In brief, fasted diabetic mice were divided into groups of six animals each. The groups were orally administered with a suspension of compounds **2** and **7** prepared in 10% Tween 80 (50 mg/kg). Glibenclamide was used as hypoglycemic reference drug (3 mg/kg). Control group was treated with 10% Tween 80. Glucose concentration was determined from mice tail at 0, 1, 3, 5, and 7 h after administration with a glucometer (Roche AccuCheck Performa, Mexico City, Mexico). The percentage of glycaemia was calculated by comparing a selected time glycaemia (G_x) with initial value (G_0) using the formula: %Variation of glycaemia = $[(G_x - G_0)/G_0] \times 100$. All values are expressed as mean ± SEM. Statistical significance was estimated by analysis of variance (ANOVA), $p < .05$ and $p < .01$ implies significance.

2.7 | Docking

Compounds **1**-**7** were docked with the crystallographic structure of PTP-1B obtained from Protein Data Bank (PDB code 1C83) resolution

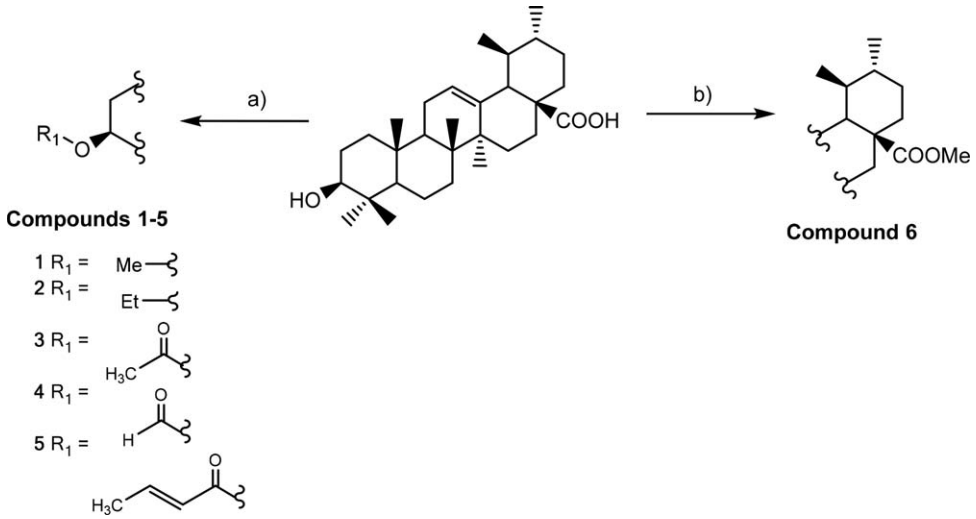

SCHEME 1 Reagents and conditions for the synthesis of ursolic acid derivatives: (a) base, 0°C, CH_2Cl_2 or THF; then acyl/alkyl halide, MW irradiation, reflux. (b) K_2CO_3, 0°C, CH_2Cl_2; then methyl iodide, MW irradiation, reflux

of 1.8, and co-crystallized with 6-(oxalylamino)-1H-indole-5-carboxilic acid. Docking studies were developed by selecting the A and B sites, described as important regions for PTP-1B inhibition (Ramírez-Espinosa et al., 2011). The A site or catalytic site is conformed by Asp181, Cys215, and Arg221, also Lys120, Ser216, Phe182, Gly220, all of them are important residues for interaction; meanwhile the region B or extended binding site is composed by Arg24, Arg254, Gln262, Tyr46, Asp48, Val49, Ile219, and Met258.

Docking calculations were conducted with AutoDock 4.2, the auxiliary program AutoGrid generate the grid maps centered at $X = 48.136$, $Y = 7.931$, and $Z = 2.961$, and the grid dimensions were $60 \times 60 \times 60$ with points separated by 0.375 for including both sites.

Before docking experiments, the protocol was validated by docking the co-crystalized ligand 6-(oxalylamino)-1H-indole-5-carboxilic acid and obtaining a RMSD of 0.33. Briefly, AutoDock performs an automated docking of the ligand with user-specified dihedral flexibility within a protein rigid binding site. The program performs several runs in each docking experiment, each run provides one predicted binding mode. All water molecules and 6-(oxalylamino)-1H-indole-5-carboxilic acid were removed from the crystallographic structure, and all hydrogen atoms were added. For all ligands and protein, Gasteiger charges were assigned and nonpolar hydrogen atoms were merged, all torsions were allowed to rotate during docking. Lamarkian genetic algorithm was applied for the search using default parameters.

The number of docking runs was 100, all solutions were clustered into groups with RMS lower than 1 after docking and the clusters were ranked by the lowest energy representative of each cluster. In order to describe the ligand–binding pocket interactions, the top ranked binding mode found by AutoDock in complex with the selected binding region of PTP-1B was subject to full energy minimization using MMFF94 force field. PyMOL 1.0 was used to generate the molecular surface of docking models.

3 | RESULTS AND DISCUSSION

3.1 | Chemistry

In our research, seven semisynthetic UA derivatives were prepared (Schemes 1 and 2), consisting in two ethers and three esters on C-3 hydroxyl group, the methyl ester and the corresponding alcohol from the reduction of C-28 carboxylic acid group. From them, ester and ether derivatives (compounds **1**–**6**) were prepared using microwave (MW) assisted synthesis procedure according to reports for some oleanolic and moronic acids derivatives (Cerón-Romero et al., 2016; Ramírez-Espinosa et al., 2014), and a conventional synthesis for compound **7**. The 3-acyloxy derivatives **3** and **5** were prepared through the reaction of UA with the respective acyl chlorides, meanwhile the ethers derivatives (**1** and **2**) and the ursolic acid methyl ester (**6**) were obtained by reaction with alkyl halide, in the presence of the corresponding base. Compound **4** was prepared by reaction between DMF in presence of benzoyl chloride as catalyst through Vilsmeier reaction. These reactions were subjected to microwave irradiation at 60°C. This methodology allowed an improved performance in the reaction times, that is, less than 3 h, although the yields were variable (Table 1). The derivative **7** was prepared by a conventional method, through UA reduction by use of $LiAlH_4$ in reflux conditions for 8 h. All compounds were characterized by NMR spectroscopy (Supporting Information).

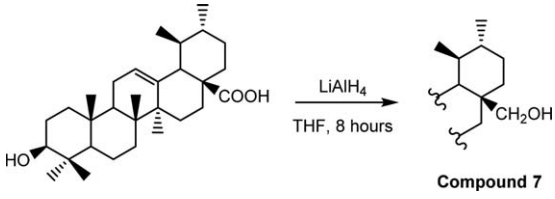

SCHEME 2 Reagents and conditions for the synthesis of derivative **7**

TABLE 1 Summary of ursolic acid derivatives synthesis

Derivative	Base	Alkyl/acyl halide	MW reaction time (hours)	Yield
1	Na	Iodomethane	2	65%
2	Na	Ethyl bromide	2	89%
3	K_2CO_3	Acetyl chloride	2	48%
4	K_2CO_3	Dimethylformamide	2	58%
5	K_2CO_3	Crotonyl chloride	3	24%
6	K_2CO_3	Iodomethane	3	76%

3.2 | *In vitro* PTP-1B inhibition assay

The inhibitory properties of these compounds against PTP-1B was screened. The initial enzymatic assays were carried out at fixed concentration of *p*-nitrophenylphosphate (2.5 mM) in the presence of 25 μM of each UA derivative. As can be seen in Figure 1, compounds **3**, **5,** and **7** were the most active; in fact, they strongly inhibit 95–99% of the enzyme activity respect to the control test DMSO; meanwhile, compound **2** was a medium inhibitor (<60%). On the other hand, compounds **1**, **4,** and **6** were weaker inhibitors with enzyme inhibition values minor than 30%.

In order to obtain the IC_{50} value for each UA derivative, the enzymatic activity of PTP-1B in the presence of increasing concentrations of UA derivatives was determined (Figure 2). The normalized residual activity values were reported in graphic versus inhibition concentrations and fitted by Equation 1.

$$y = \frac{\text{Max} - \text{Min}}{1 + \left(\frac{x}{IC_{50}}\right)^{\text{slope}}} + \text{Min} \quad (1)$$

From that, it was found that **3**, **5**, and **7** were the most potent compounds (Figure 2), with IC_{50} values minor to 10 μM (Table 2); which allowed us to classify these compounds as hits, meanwhile compound **2** IC_{50} was around 20 μM. The remaining compounds exhibited IC_{50} values higher than 100 μM (graphics not shown). So, these values are similar to that described for UA (IC_{50} = 3.08 μM) (Ramírez-Espinosa et al., 2011; Zhang et al., 2006). All of these results correlate with the complete PTP-1B inhibition of the most active compounds with their corresponding low IC_{50} values, and also explain in part, the reason why the remaining compounds did not show important inhibition values over PTP-1B. Also, in a previous work with oleanolic acid derivatives, we described that is necessary the presence of the carboxylic acid and/or its corresponding reduction product carbinol derivative (H-bond donor) in C-28 to maintain the inhibitory activity (Ramírez-Espinosa et al., 2014). Thus, the fact that introducing a methyl ester in C-28 in UA to obtain compound **6**, led to a weaker inhibition of enzymatic activity in current investigation.

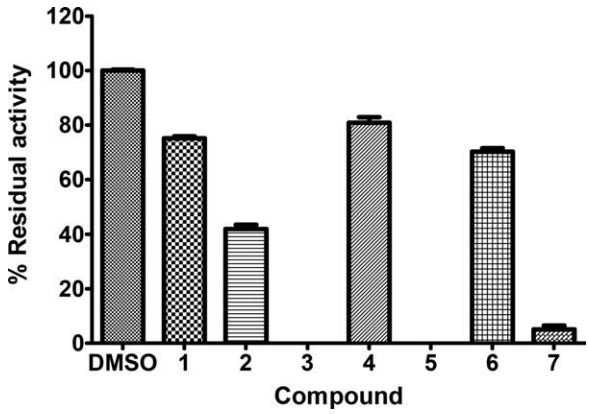

FIGURE 1 PTP-1B inhibition activity assay of UA derivatives at 25 μM. The data reported represent the mean ± SEM. All experiments were performed in triplicate

Finally, for a better understanding of the type of enzymatic inhibition, an additional reversibility tests were performed. For that, the most active derivatives were incubated with an aliquot of PTP-1B during one hour. It is known that UA inhibits in a complete reversible manner (Ramírez-Espinosa et al., 2011). From the data in Figure 3, we argued that all compounds tested were PTP-1B reversible inhibitors, because the enzyme recovered its complete *in vitro* activity after compounds were eliminated, showing a similar performance as that reported for the parent compound UA (Ramírez-Espinosa et al., 2011).

The potential of some triterpenic acids as promising PTP-1B inhibitors has been reported; however, these showed two main disadvantages: (1) they are not selective on this target, since these compounds inhibit other phosphatases, sharing 50–80% of homology with PTP-1B in their catalytic site, which represents a great challenge for to develop selective compounds; (2) they have not the same potency/activity as the parent compound UA, which also has more selectivity to PTP-1B over other phosphatases (Zhang et al., 2006). Owing to this, some UA derivatives have been developed in order to achieve better compounds. In our case, we found that three of the seven synthesized compounds showed important activity over PTP-1B with low IC_{50} values; also, the inhibition caused by these derivatives was reversible. This is important since the irreversible inhibition of PTP-1B may cause overstimulation of insulin receptor, which finally can lead the desensitization of the receptor and/or side effects such as a drastic hypoglycemic effect.

To date, only one of the UA derivatives with significant antidiabetic effect has been reported, named UA0713, mediating PTP-1B inhibition (Zhang et al., 2006). However, this compound was not a selective enzymatic inhibitor, because it displayed similar IC_{50} values among PTP-1B and other phosphatases.

3.3 | Molecular docking with PTP-1B

In order to gain insight into the putative binding mode of compounds **1**–**7** with PTP-1B, their structures were docked with a crystallographic structure of human PTP-1B, which was obtained from the Protein Data Bank (accession code 1C83). Before docking the UA derivatives, the protocol was validated by predicting the binding mode of 6-(oxalylamino)-1*H*-indole-5-carboxilic acid, a competitive inhibitor of PTP-1B. Figure 4 shows a comparison between binding mode of the crystallographic ligand and the mode predicted by AutoDock. This figure clearly shows that AutoDock successfully predicted the binding mode of

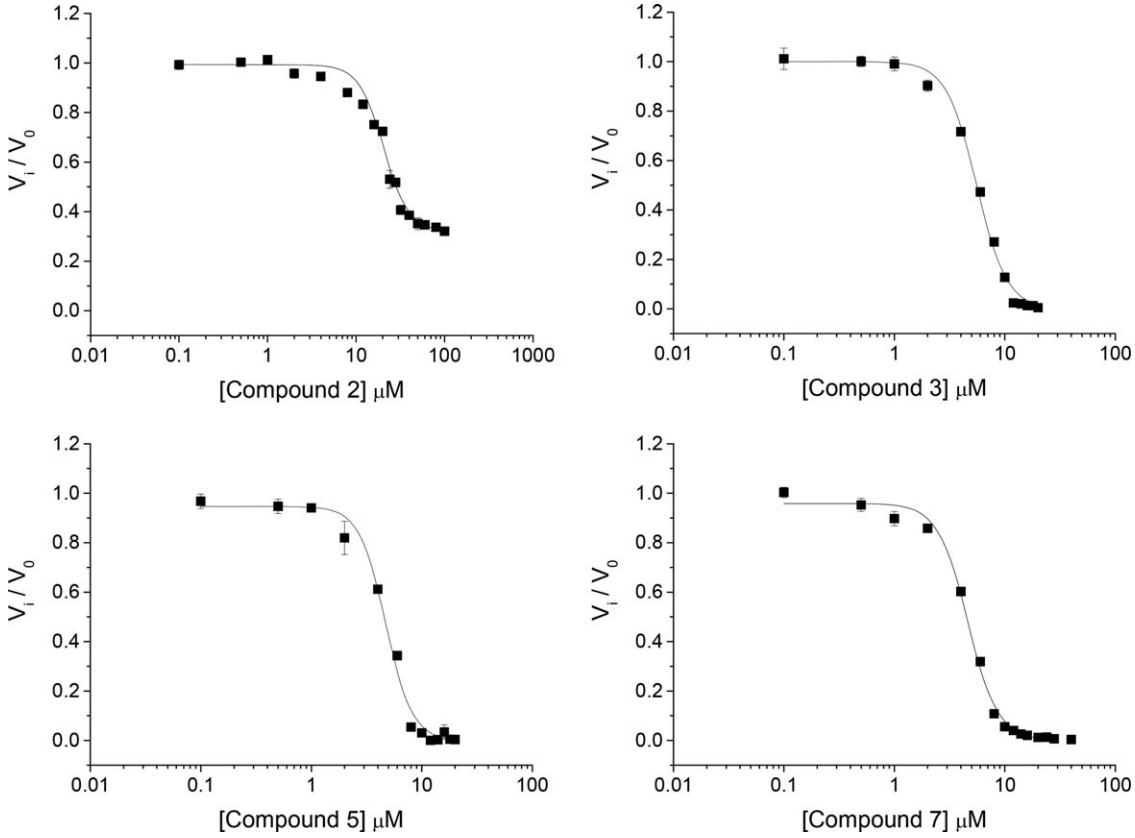

FIGURE 2 IC_{50} determination for derivatives **2**, **3**, **5**, and **7**. These values were determined by plotting the data relative to the residual activity of PTP-1B against the inhibitor concentration. 10–15 different inhibitor concentrations were used for every derivative. All assays were performed in quadruplicate. Data represent the mean ± SEM [Color figure can be viewed at wileyonlinelibrary.com]

crystallographic ligand with a root-mean square deviation (RMSD) of 0.33 Å. Predicted Binding energies, Ki's and binding sites determined by AutoDock for the seven compounds are summarized in Table 3. As it can be seen, compounds **3** and **5** showed the better Δ°G and Ki's calculated, which clearly correlates with its binding location that is the catalytic site. Moreover, both **3** and **5** were two of the three most *in vitro* active compounds of the entire series. Therefore, there exist an important correlation between docking prediction interactions with *in vitro* inhibitory activity on PTP-1B. In this context, the remaining compounds interacted with the extended B-binding site, and their Δ°*G* and Ki's calculated were less than the most active compounds **3** and **5**, subsequently, the *in vitro* inhibitory activity shown by **1**, **2**, **4**, and **6** were weaker or inactive. With exception of compound **7** that showed

TABLE 2 Assay for reversibility of inhibition and IC_{50} values against PTP-1B

Compound	% Reversibility	IC_{50} (μM)
DMSO	100.0 ± 9.8	–
1	n.t.	>100
2	94.3 ± 0.5	20.6 ± 0.2
3	96.3 ± 5.0	5.6 ± 0.2
4	n.t.	>100
5	99.8 ± 1.0	4.7 ± 0.2
6	n.t.	>100
7	88.3 ± 1.1	4.6 ± 0.2

The data reported represent the value ± SEM of triplicates.
n.t., not tested.

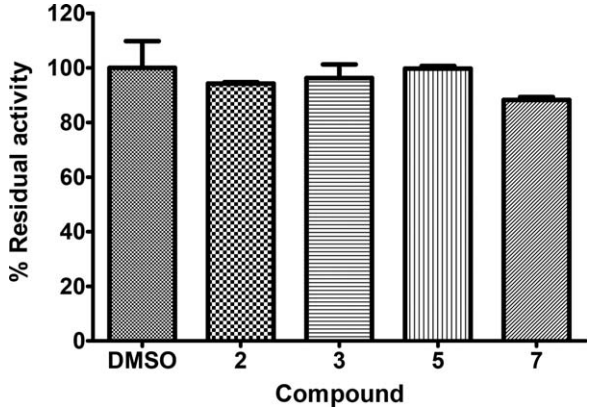

FIGURE 3 Inhibition reversibility test. PTP-1B aliquots were incubated in presence of fixed concentration of each compound for 1 h at 37°C, then the enzyme was diluted with assay solution to measure the residual activity [Color figure can be viewed at wileyonlinelibrary.com]

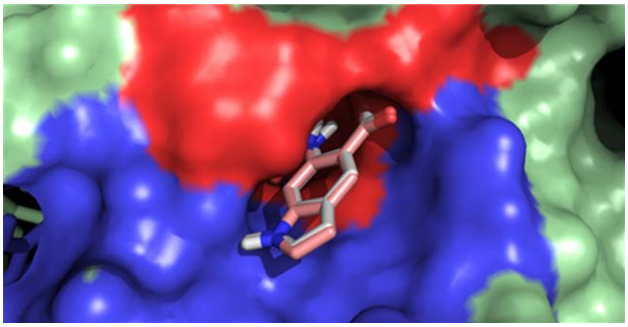

FIGURE 4 Surface representation of the binding sites of PTP-1B. Catalytic binding site or site A, is shown in red, extended binding site B is in blue. A comparison between the binding position of the co-crystal ligand (gray) and the binding position predicted by Auto-Dock (pink) is also shown (RMSD = 0.33 Å) [Color figure can be viewed at wileyonlinelibrary.com]

interactions with extended site B with $\Delta°G$ = −6.43 Kcal/mol and Ki = 18 μM, however, was one of the most active compound in *in vitro* inhibition. Further *in silico* experiments are necessary to clarify this result.

To illustrate different predicted ways in which compound **3** (catalytic site) and **7** (extended binding site) are interacting with PTP-1B, in Figures 5–8 are shown their interactions. Docking score of derivatives with PTP-1B active site A and extended binding site B, showed that **3** (Figures 5 and 7) had polar and Van der Waals interactions in both sites with Lys120, Tyr46, Ser216, Ala217, Ile219, Asp181, Phe182, Gln262, Val49, Met258, and Gly259, showing a docking score value of −7.48 kcal/mol, being more specific for site B, explaining the reversible inhibition of PTP-1B. On the other hand, Compound **7** (Figures 6 and 8) showed polar interaction with Gln262 and Van der Waals with Ala217, Phe182, Ile219, Arg45, Tyr46, Arg47, Asp48, and Val49 with a predictive docking score of −6.43 kcal/mol, suggesting that the potential binding site could be localized in an extended binding pocket (site B) adjacent to the catalytic site A. The fact that compound **7** showed interactions with extended binding site B, and the docking score value could explain the lesser experimental PTP-1B inhibition percentage in comparison to compound **3**.

TABLE 3 Predicted binding site, docking score, and affinity constant for UA and compounds **1–7** over PTP-1B

Compound	Binding site	$\Delta°G$ (kcal/mol)	*Ki* (μM)
UA	Allosteric (extended)	−7.15	5.49
1	Allosteric (extended)	−6.82	9.96
2	Allosteric (extended)	−6.72	11.88
3	Catalytic	−7.48	3.14
4	Allosteric (extended)	−7.03	7.0
5	Catalytic	−8.23	0.88
6	Allosteric (extended)	−7.16	5.67
7	Allosteric (extended)	−6.43	18.06

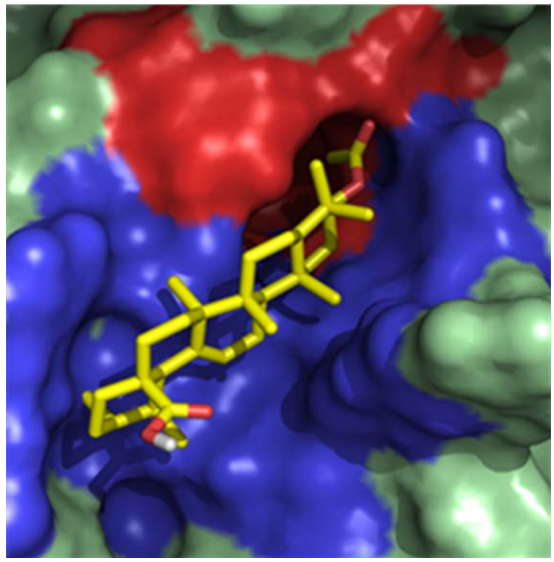

FIGURE 5 3D binding mode of compound **3** [Color figure can be viewed at wileyonlinelibrary.com]

3.4 | *In vivo* antidiabetic effect

Based on the PTP-1B IC_{50} values and inhibitory pattern, compounds **2** and **7** were selected to be evaluated through acute evaluation, on experimental noninsulin diabetic mice model (Figure 9). Compound **7** was selected because of its potent IC_{50} value and its pattern as a nearly complete PTP-1B inhibitor, whilst derivative **2** was tested since its PTP-1B inhibition was moderated, in order to prove the potential correlation between *in vitro* and *in vivo* experiments.

The acute administration of 50 mg/kg of **7** showed a significant decrease in the variation of glycaemia ($p < .05$) from the first hour, and this effect was sustained until the end of the assay (7 h). This hypoglycemic effect over 70% was similar to the control drug glibenclamide,

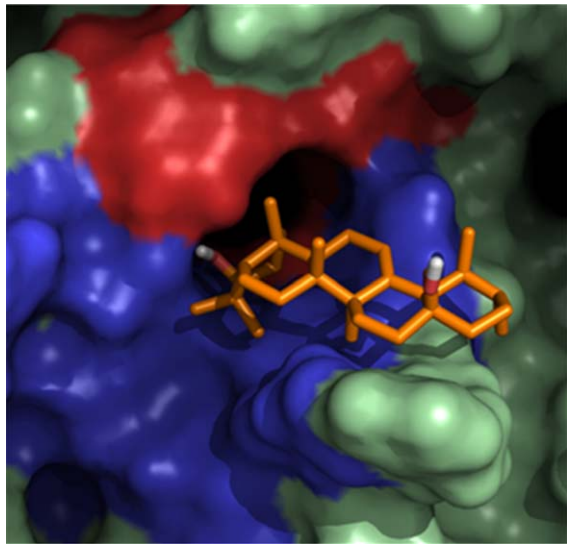

FIGURE 6 3D binding mode of compound **7** [Color figure can be viewed at wileyonlinelibrary.com]

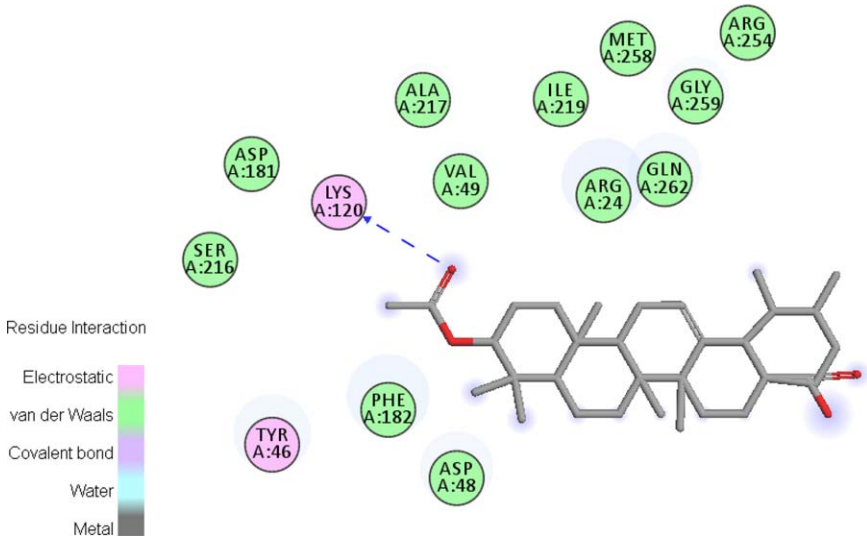

FIGURE 7 Two-dimensional interaction diagram of the predicted binding mode of **3** with PTP-1B [Color figure can be viewed at wileyonlinelibrary.com]

and better than the parent compound UA. Meanwhile, compound **2** did not show a significant effect within the three first hours of the acute assay; however, an important hypoglycemic effect was determined after fifth hour and until the end of the experiment, achieving a hypoglycemic effect value around 55%.

From these results, we conclude that derivative **7** presents a better *in vivo* acute hypoglycemic effect in comparison with **2**. This observation can be explained by two points: (1) the derivative **7** IC_{50} value was lower than **2**, which means a better potency and inhibition of PTP-1B by compound **7**, and therefore better sensibility to insulin action in the corresponding treated animals; and (2) it is proposed that **2** could be a prodrug, that is why we mentioned that the delayed effect (i.e., after 3 h of administration an effect was observed) could be due if **2** acts as a prodrug, this because after metabolism it could be transformed into UA, and then UA exerts its antidiabetic action; however, we have not explored that possibility yet. A similar approach has been reported with a different compound by Boutselis, Yu, Zhang, and Borch (2007). It is important to show that both compounds had better pattern that the parent compound UA, and this poor hypoglycemic effect over this NIDDM model could be due to poor gut absorption.

4 | CONCLUSION

We prepared seven ursolic acid semisynthetic derivatives. Six compounds were prepared by microwave-assisted synthesis method, which allowed to improve reaction times although yields were variable. Compounds **3**, **5**, and **7** showed significant inhibitory activity on PTP-1B enzyme in a reversible manner. The most active compound was **7** showing important *in vitro* and *in vivo* effects. Furthermore, acetyl and crotonyl esters were the most active derivatives through *in vitro*

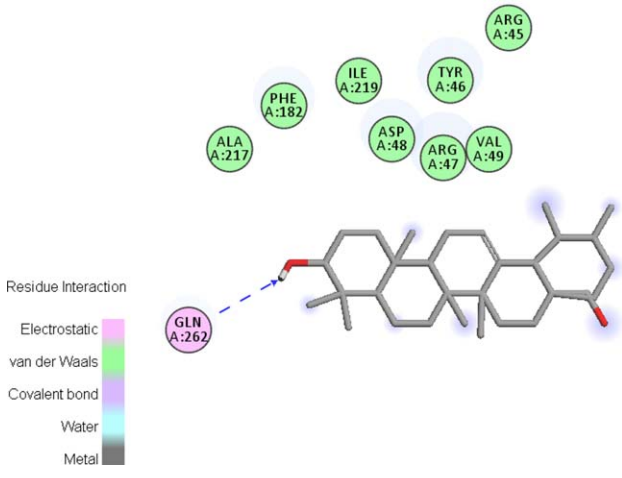

FIGURE 8 Two-dimensional interaction diagram of the predicted binding mode of compound **7** with PTP-1B [Color figure can be viewed at wileyonlinelibrary.com]

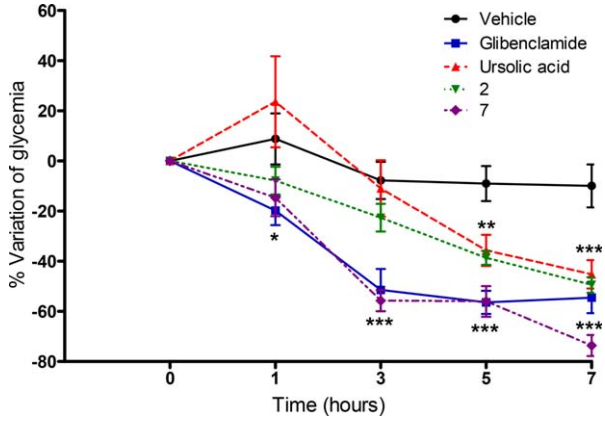

FIGURE 9 Percentage of variation of blood glucose concentration on noninsulin dependent diabetic mice model treated with UA, 2 or 7. Values represent the mean ± SEM ($n = 6$). *$p < .05$ compared with control group [Color figure can be viewed at wileyonlinelibrary.com]

studies; however, further experiments are necessary to determine the *in vivo* effects for these compounds. The molecular docking studies showed that acetyl and crotonyl derivatives had better binding scores compared to the parent compound, ursolic acid.

ACKNOWLEDGMENTS

This study was supported by Consejo Nacional de Ciencia y Tecnología (CONACyT) Proyecto de Ciencia Básica 167044. R. Guzmán-Ávila is grateful with CONACyT for the Pharm. M. fellowship grant. Taken in part from the Master in Pharmacy of R. Guzmán-Ávila.

CONFLICT OF INTEREST

The authors report no conflicts of interest.

AUTHOR CONTRIBUTIONS

Study design, coordination and *in vivo* studies: S. Estrada-Soto, R. Villalobos-Molina, L. Cerón-Romero; J.J. Ramírez-Espinosa; *in vitro* PTP-1B inhibition: G. Camici and P. Paoli; preparation of the UA derivatives, purification and structural elucidation; V. Flores-Morales; M.Y. Rios and R. Guzmán-Ávila; in silico studies G. Navarrete-Vázquez; S. Hidalgo-Figueroa and R. Guzmán-Ávila; preparation and writing of the manuscript R. Guzmán-Ávila, S. Estrada-Soto, and R. Villalobos-Molina; Finally, all authors contributed to the writing and revised the manuscript.

ORCID

Virginia Flores-Morales http://orcid.org/0000-0003-4540-1011
Samuel Estrada-Soto http://orcid.org/0000-0003-1860-0744
Gabriel Navarrete-Vázquez http://orcid.org/0000-0001-5344-4762

REFERENCES

Aguirre-Crespo, F., Vergara-Galicia, J., Villalobos-Molina, R., López-Guerrero, J. J., Navarrete-Vázquez, G., & Estrada-Soto, S. (2006). Ursolic acid mediates the vasorelaxant activity of *Lepechinia caulescens* via NO release in isolated rat thoracic aorta. *Life Science*, *79*, 1062–1068.

Allouche, Y., Beltrán, G., Gaforio, J. J., Uceda, M., & Mesa, M. D. (2010). Antioxidant and antiatherogenic activities of pentacyclic triterpenic diols and acids. *Food Chemical & Toxicology*, *48*, 2885–2890.

Boutselis, I. G., Yu, X., Zhang, Z. Y., & Borch, R. F. (2007). Synthesis and cell-based activity of a potent and selective protein tyrosine phosphatase 1B inhibitor prodrug. *Journal of Medical Chemistry*, *50*, 856–864.

Brownlee, M. (2001). Biochemistry and molecular cell biology of diabetic complications. *Nature*, *414*, 813–820.

Castro, A. J. G., Frederico, M. J. S., Cazarolli, L. H., Mendes, C. P., Bretanha, L. C., Schmidt, É. C., … Silva, F. R. M. B. (2015). The mechanism of action of ursolic acid as insulin secretagogue and insulinomimetic is mediated by cross-talk between calcium and kinases to regulate glucose balance. *Biochemical Biophysical Acta*, *1850*, 51–61.

Cerón-Romero, L., Paoli, P., Camici, G., Flores-Morales, V., Rios, M. Y., Ramírez-Espinosa, J. J., … Estrada-Soto, S. (2016). *In vitro* and *in silico* PTP-1B inhibition and *in vivo* antidiabetic activity of semisynthetic moronic acid derivatives. *Bioorganic Medicine & Chemical Letters*, *26*, 2018–2022.

Chávez-Silva, F., Cerón-Romero, L., Arias-Durán, L., Navarrete-Vázquez, G., Almanza-Pérez, J., Román-Ramos, R., … Estrada-Soto, S. (2018). Antidiabetic effect of *Achillea millefollium* through multitarget interactions: α-glucosidase inhibition, insulin sensitization and insulin secretagogue activities. *Journal of Ethnopharmacology*, *212*, 1–7.

Colla, A. R. S., Oliveira, Á., Pazini, F. L., Rosa, J. M., Manosso, L. M., Cunha, M. P., & Rodrigues, A. L. S. (2014). Serotonergic and noradrenergic systems are implicated in the antidepressant-like effect of ursolic acid in mice. *Pharmacology Biochemical & Behaviour*, *124*, 108–116.

Collins, D. O., Ruddock, P. L. D., Chiverton, J., Grasse, D., Reynolds, W. F., & Reese, P. B. (2002). Microbial transformation of cadina-4,10 (15)-dien-3-one, aromadendr-1(10)-en-9-one and methyl ursolate by Mucor plumbeus ATCC 4740. *Phytochemistry*, *59*, 479–488.

Hidalgo Figueroa, S., Navarrete-Vázquez, G., Estrada-Soto, S., Giles-Rivas, D., Alarcón-Aguilar, F. J., León-Rivera, I., … Almanza-Pérez, J. (2017). Discovery of new dual PPAR γ-GPR40 agonists with robust antidiabetic activity: Design, synthesis and *in combo* drug evaluation. *Biomedical Pharmacotherapy*, *90*, 53–61.

Innocente, A., Casanova, B. B., Klein, F., Lana, A. D., Pereira, D., Muniz, M. N., … Gnoatto, S. C. B. (2014). Synthesis of isosteric triterpenoid derivatives and antifungal activity. *Chemical Biology & Drug Design*, *83*, 344–349.

Jang, S. M., Kim, M. J., Choi, M. S., Kwon, E. Y., & Lee, M. K. (2010). Inhibitory effects of ursolic acid on hepatic polyol pathway and glucose production in streptozotocin-induced diabetic mice. *Metabolism*, *59*, 512–519.

Johnson, T. O., Ermolieff, J., & Jirousek, M. R. (2002). Protein tyrosine phosphatase 1B inhibitors for diabetes. *Nature Review & Drug Discovery*, *1*, 696–709.

Jung, S. H., Ha, Y. J., Shim, E. K., Choi, S. Y., Jin, J. L., Yun-Choi, H. S., & Lee, J. R. (2007). Insulin-mimetic and insulin-sensitizing activities of a pentacyclic triterpenoid insulin receptor activator. *Biochemical Journal*, *250*, 243–250.

Klok, M. D., Jakobsdottir, S., & Drent, M. L. (2007). The role of leptin and ghrelin in the regulation of food intake and body weight in humans: A review. *Obesity Review*, *8*, 21–34.

Lee, J., Lee, H., Seo, K., Cho, H. W., Kim, M., Park, E., & Lee, M. (2014). Effects of ursolic acid on glucose metabolism, the polyol pathway and dyslipidemia in non-obese type 2 diabetic mice. *Indian Journal of Experimental Biology*, *52*, 683–691.

Li, Y., Lu, X., Qi, H., Li, X., Xiao, X., & Gao, J. (2014). Ursolic acid induces apoptosis through mitochondrial intrinsic pathway and suppression of ERK1/2 MAPK in HeLa cells. *Journal of Pharmacology Science*, *125*, 202–210.

Li, Z., Zhang, W., & Sima, A. A. F. (2007). Diabetes. *Biomedical Research*, *56*, 1817–1824.

Liu, Q., Chen, L., Hu, L., Guo, Y., & Shen, X. (2010). Small molecules from natural sources, targeting signaling pathways in diabetes. *Biochimical Biophysical Acta*, *1799*, 854–865.

Machado, D. G., Neis, V. B., Balen, G. O., Colla, A., Cunha, M. P., Dalmarco, J. B., … Rodrigues, A. L. S. (2012). Antidepressant-like effect of ursolic acid isolated from *Rosmarinus officinalis* L. in mice: Evidence for the involvement of the dopaminergic system. *Pharmacology Biochemical & Behaviour*, *103*, 204–211.

Mahapatra, D. K., Asati, V., & Bharti, S. K. (2015). Chalcones and their therapeutic targets for the management of diabetes: Structural and pharmacological perspectives. *European Journal of Medical Chemistry*, *92*, 839–865.

Nascimento, P. G. G., Lemos, T. L. G., Bizerra, A. M. C., Arriaga, Â. M. C., Ferreira, D. A., Santiago, G. M. P., ... Costa, J. G. M. (2014). Antibacterial and antioxidant activities of ursolic acid. *Molecules*, *19*, 1317–1327.

Puius, Y. A., Zhao, Y., Sullivan, M., Lawrence, D. S., Almo, S. C., & Zhang, Z. Y. (1997). Identification of a second aryl phosphate-binding site in protein-tyrosine phosphatase 1B: a paradigm for inhibitor design. *Proceedings of National Academic Sciences USA*, *94*, 13420–13425.

Ramírez-Espinosa, J. J., Rios, M. Y., López-Martínez, S., López-Vallejo, F., Medina-Franco, J. L., Paoli, P., ... Estrada-Soto, S. (2011). Antidiabetic activity of some pentacyclic acid triterpenoids, role of PTP–1B: *In vitro*, *in silico*, and *in vivo* approaches. *European Journal of Medical Chemistry*, *46*, 2243–2251.

Ramírez-Espinosa, J. J., Rios, M. Y., Paoli, P., Flores-Morales, V., Camici, G., La Rosa-Lugo, V. D., ... Estrada-Soto, S. (2014). Synthesis of oleanolic acid derivatives: *In vitro*, *in vivo* and *in silico* studies for PTP-1B inhibition. *European Journal of Medical Chemistry*, *87*, 316–327.

Rios, M. Y., López-Martínez, S., López-Vallejo, F., Medina-Franco, J. L., Villalobos-Molina, R., Ibarra-Barajas, M., ... Estrada-Soto, S. (2012). Vasorelaxant activity of some structurally-related triterpenic acids from *Phoradendron reichenbachianum* (Viscaceae) mainly by NO production: *ex vivo* and *in silico* studies. *Fitoterapia*, *83*, 1023–1029.

Rollinger, J. M., Kratschmar, D. V., Schuster, D., Pfisterer, P. H., Gumy, C., Aubry, E. M., ... Odermatt, A. (2010). 11β-Hydroxysteroid dehydrogenase 1 inhibiting constituents from Eriobotrya japonica revealed by bioactivity-guided isolation and computational approaches. *Bioorganic Medical Chemistry*, *18*, 1507–1515.

Romsicki, Y., Reece, M., Gauthier, J. Y., Asante-Appiah, E., & Kennedy, B. P. (2004). Protein tyrosine phosphatase dephosphorylation of the insulin receptor occurs in a perinuclear endosome compartment in human embryonic kidney 293 cells. *Journal of Biological Chemistry*, *279*, 12868–12875.

Sheng, H., & Sun, H. (2011). Synthesis, biology and clinical significance of pentacyclic triterpenes: a multi-target approach to prevention and treatment of metabolic and vascular diseases. *Nature Products & Reports*, *28*, 543–593.

Somova, L. O., Nadar, A., Rammanan, P., & Shode, F. O. (2003a). Cardiovascular, antihyperlipidemic and antioxidant effects of oleanolic and ursolic acids in experimental hypertension. *Phytomedicine*, *10*, 115–121.

Somova, L. I., Shode, F. O., Ramnanan, P., & Nadar, A. (2003b). Antihypertensive, antiatherosclerotic and antioxidant activity of triterpenoids isolated from Olea europaea, subspecies africana leaves. *Journal of Ethnopharmacology*, *84*, 299–305.

Tahrani, A. A., Bailey, C. J., Del Prato, S., & Barnett, A. H. (2011). Management of type 2 diabetes: New and future developments in treatment. *Lancet*, *378*, 182–197.

Tonks, N. K. (2003). PTP1B: From the sidelines to the front lines! *FEBS Letters*, *546*, 140–148.

Verma, M., Gupta, S. J., Chaudhary, A., & Garg, V. K. (2017). Protein tyrosine phosphatase 1B inhibitors as antidiabetic agents: A brief review. *Bioorganic Chemistry*, *70*, 267–283.

Wu, P. P., Zhang, K., Lu, Y. J., He, P., & Zhao, S. Q. (2014). *In vitro* and *in vivo* evaluation of the antidiabetic activity of ursolic acid derivative. *European Journal of Medical Chemistry*, *80*, 502–508.

Zhang, W., Hong, D., Zhou, Y., Zhang, Y., Shen, Q., Li, J.-Y., ... Li, J. (2006). Ursolic acid and its derivative inhibit protein tyrosine phosphatase 1B, enhancing insulin receptor phosphorylation and stimulating glucose uptake. *Biochimical Biophysical Acta*, *1760*, 1505–1512.

SUPPORTING INFORMATION

Additional Supporting Information may be found online in the supporting information tab for this article.

How to cite this article: Guzmán-Ávila R, Flores-Morales V, Paoli P, et al. Ursolic acid derivatives as potential antidiabetic agents: *In vitro*, *in vivo*, and *in silico* studies. *Drug Dev. Res.* 2018;00:1–11. https://doi.org/10.1002/ddr.21422